

Dielectric and magnetic properties of BiFe_{1-4x/3}Ti_xO₃ ceramics with iron vacancies: Experimental and first-principles studies

L. Y. Zou, R. P. Yang, Y. B. Lin, M. H. Qin, X. S. Gao et al.

Citation: *J. Appl. Phys.* **114**, 034105 (2013); doi: 10.1063/1.4813784

View online: <http://dx.doi.org/10.1063/1.4813784>

View Table of Contents: <http://jap.aip.org/resource/1/JAPIAU/v114/i3>

Published by the [AIP Publishing LLC](#).

Additional information on J. Appl. Phys.

Journal Homepage: <http://jap.aip.org/>

Journal Information: http://jap.aip.org/about/about_the_journal

Top downloads: http://jap.aip.org/features/most_downloaded

Information for Authors: <http://jap.aip.org/authors>

ADVERTISEMENT



AIPAdvances

Now Indexed in Thomson Reuters Databases

Explore AIP's open access journal:

- Rapid publication
- Article-level metrics
- Post-publication rating and commenting

Dielectric and magnetic properties of $\text{BiFe}_{1-4x/3}\text{Ti}_x\text{O}_3$ ceramics with iron vacancies: Experimental and first-principles studies

L. Y. Zou,¹ R. P. Yang,¹ Y. B. Lin,¹ M. H. Qin,¹ X. S. Gao,¹ M. Zeng,^{1,a)} and J.-M. Liu^{1,2,b)}

¹Institute for Advanced materials, South China Normal University, Guangzhou 510006, China

²Laboratory of Solid State Microstructures, Nanjing University, Nanjing 210093, China

(Received 14 April 2013; accepted 25 June 2013; published online 18 July 2013)

$\text{BiFe}_{1-4x/3}\text{Ti}_x\text{O}_3$ ($x = 0-0.2$) ceramics with Fe vacancies created by nonstoichiometric compositions were synthesized to study their crystal structures, dielectric, and ferromagnetic behaviors. X-ray diffraction and Raman spectroscopy analysis reveal a structure transition from rhombohedral to orthorhombic phases at $x = 0.2$. Dielectric measurement shows that the dielectric loss is significantly reduced in the Ti-doped BiFeO_3 samples. With increasing x concentration, the remanent magnetization (M_r) first increases and then decreases. The maximal M_r of 0.13 emu/g is obtained at $x = 0.05$. Furthermore, theoretical calculations based on the density-functional theory prove that the Ti-doping does enhance the lattice constants, band gap, and magnetization. These results show that the Ti-doped BiFeO_3 with Fe vacancies could enhance resistivity and magnetism, implying a possible improvement in multiferroic behavior. © 2013 AIP Publishing LLC.

[<http://dx.doi.org/10.1063/1.4813784>]

I. INTRODUCTION

Multiferroic materials that exhibit both ferroelectric and ferromagnetic properties simultaneously are a time-honored research subject due to their interesting fundamental physics as well as potential applications in devices.¹⁻³ Single-phase BiFeO_3 (BFO) ceramic, processed antiferromagnetic ordering with Neel temperature $T_N \sim 643$ K and ferroelectric ordering with Curie temperature $T_C \sim 1103$ K, is the most extensively studied room temperature multiferroic materials.⁴⁻¹⁰ The large ferroelectric polarization ($\sim 100 \mu\text{C}/\text{cm}^2$), exceeding those of prototypical ferroelectrics BaTiO_3 and PbTiO_3 , has been reported in BFO thin film and single crystal forms, and is mainly originated from the Bi atom off-center distortion.³⁻⁵ On the other hand, its magnetism is very weak in the macroscopic size due to its antiferromagnetic ordering modulated by the incommensurate sinusoidal spin arrangement of which the wavelength is 620 \AA .⁶

Although BFO exhibits a large ferroelectric polarization, the applications of BFO bulk ceramics are limited by some inherent problems, such as the preparation of a pure phase compound, the high leakage current density and weak ferromagnetism.¹⁰⁻¹⁷ The appearance of parasitic phases is attributed to the low chemical stability due to the volatilization of Bi_2O_3 , and the high leakage current density mainly originates from the oxygen vacancies induced valence fluctuation of iron ions (Fe^{3+} to Fe^{2+}).^{8,9} In the past decades, many methods have been attempted in order to overcome these drawbacks. On the one hand, some specific synthesis techniques such as rapid liquid phase sintering or leaching the impurity phase with dilute nitric acid is proven to be an effective method to fabricate a pure phase BFO ceramics with improving resistivity.^{11,16} On the other hand, the chemical substitution of A- or/and B-sites ions by other elements

has been undertaken extensively for improving the multiferroic properties.¹²⁻¹⁷ For examples, the enhanced dielectric constant, the improving leakage current density and ferroelectric polarization have been reported in BFO ceramics by the partial substitution of Bi^{3+} ions by the rare earth elements such as La^{3+} , Dy^{3+} , and Tb^{4+} .^{12,13} Also, the enhanced ferromagnetism has been revealed in BFO ceramics with the partial substitution of Fe^{3+} ions by the Ga^{3+} , Ti^{4+} , and Mn^{4+} .¹⁴⁻¹⁷

Among of those doping reported, aliovalent ions with non-magnetic such as Ti^{4+} , which have a similar ion size with Fe^{3+} , seem especially attractive. The addition of Ti^{4+} ions to BFO was believed to not only maintain the structural stability with ferroelectric properties but also suppress the AFM spin ordering. In other words, Ti substitution is promising for simultaneously solving two main problems: the leakage current density and weak magnetism. A decreased resistivity by three orders of magnitude upon 2% Ti-substituted BFO film and an improved resistivity and enhanced magnetization in Ti-doped BFO ceramics are reported.¹⁸ Generally, the substitution of Fe^{3+} ions by Ti^{4+} ions in BFO requires charge compensation, which leads to the formation of Fe^{2+} or the creation of cation/oxygen vacancies. Consequently, the multiferroic properties are influenced greatly. However, most studies have been focused on the stoichiometric compositions, i.e., the ratio of Fe^{3+} to Ti^{4+} is 1:1, while the study on Ti-doped BFO ceramics with nonstoichiometric compositions and charge neutrality, such as chemical formula $\text{BiFe}_{1-4x/3}\text{Ti}_x\text{O}_3$, is lack. Actually, in these ceramics, Fe vacancies may be created from the viewpoint of lattice site occupation as reported in the nonstoichiometric compositions (the ratio of Fe^{3+} to Ti^{4+} is 2:1). It can be expected that Fe vacancies have direct effects on the AFM spin orderings in BFO so that the magnetic along with ferroelectric behaviors will be significantly different from the one in pure BFO. Thus, a detailed investigation on the

^{a)}E-mail: zengmin@scnu.edu.cn.

^{b)}E-mail: liujm@nju.edu.cn.

role of Fe vacancies in Ti-doped BFO ceramic is needed. In this paper, we performed a comprehensive study of the $\text{BiFe}_{1-4x/3}\text{Ti}_x\text{O}_3$ ceramics by combining experiment theoretical calculation. It was found that Fe vacancies play a vital role in the suppression of the cycloid AFM spin orderings, leading to an obviously enhanced magnetism and improved resistivity, while the ferroelectric polarization is not degraded. This implies a possible improvement in multiferroic behavior in Ti-doped BFO ceramics with Fe vacancies.

II. EXPERIMENTAL DETAILS

$\text{BiFe}_{1-4x/3}\text{Ti}_x\text{O}_3$ ($x=0-0.2$) ceramics were prepared by high-energy ball milling method. High purity Bi_2O_3 , Fe_2O_3 , and TiO_2 powder were carefully weighed according to the chemical compositions and fully dry-mixed by high-energy ball milling for 8 h. After ball milling, the mixture powders were uniaxially pressed into pellets with 10 mm in diameter, and 1 mm thickness by applying a pressure of 8 MPa. To obtain pure phase samples with possible high electrical resistivity, a series of sintered temperature between 800 and 1000 °C were tested in all samples. Finally, an optimum condition with sintered temperature 850 °C for 2 h was chosen. The crystal structures of the samples were characterized by x-ray diffraction (XRD) (PANalytical X' Pert PRO diffractometer). Raman spectroscopy was determined using inVia-Reflex micro-Raman system with 633 nm Ar ion laser source in backscattering geometry. Dielectric measurements were carried out through high performance frequency analyzer (Alpha-A, Novocontrol Technology) with frequency range of 10^{-1} to 10 MHz at room temperature. The magnetic properties were evaluated by a vibrating sample magnetometer incorporated into a physical properties measurement system (PPMS).

III. RESULTS AND DISCUSSION

Figure 1 shows the x-ray diffraction (XRD) patterns of the $\text{BiFe}_{1-4x/3}\text{Ti}_x\text{O}_3$ ceramics ($x=0-0.2$). It can be found that the sintered ceramics exhibit well crystallized diffraction

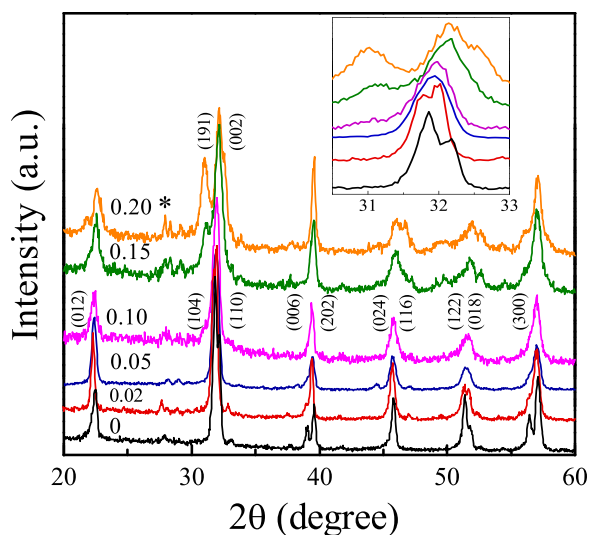


FIG. 1. X-ray diffraction patterns for the $\text{BiFe}_{1-4x/3}\text{Ti}_x\text{O}_3$ ceramics ($x=0-0.2$). The asterisk denotes the impure phase $\text{Bi}_2\text{Fe}_4\text{O}_9$.

patterns along with some minor impure phases. For the pure BFO ($x=0$), the diffraction peaks can be identified as a rhombohedrally distorted perovskite structure with a space group of $R3c$. With increasing x , the (110)/(104) peak around 32° , see the inset of Fig. 1, shifts towards the lower angle up to $x=0.1$, indicating that Ti doping induces an expanded lattice constant. Similar results were previously reported in other doped BFO systems such as $\text{Bi}_{0.9-x}\text{Tb}_x\text{La}_{0.1}\text{FeO}_3$, $\text{BiFe}_{1-x}\text{Mn}_x\text{O}_3$, $\text{BiFe}_{1-x}\text{Ti}_x\text{O}_3$.¹⁴⁻¹⁶ Further increasing x , a small amount of secondary phases occur. The parasitic phase is characterized as $\text{Bi}_2\text{Fe}_4\text{O}_9$. In particular, some (119) and (002) peaks around 32° are presented at $x > 0.15$. It is worthy noting that the XRD patterns at $x=0.2$ reveal the formation of the orthorhombic crystal structure, corresponding to the chemical formula $\text{Bi}_{15}\text{Fe}_{11}\text{Ti}_3\text{O}_{45}$. This means that the Ti-doping results in a clearly structural transition from rhombohedral to orthorhombic phases at $x=0.2$. Similar phenomenon has been reported previously in Ti-doped BFO ceramics with stoichiometric composition, in which the structure transition was observed at $x=0.33$.¹⁴ In contrast, this structure transition occurred at $x=0.2$ can be attributed to the introduction of Fe vacancies in our samples.

Figure 2 plots the room temperature Raman spectra of $\text{BiFe}_{1-4x/3}\text{Ti}_x\text{O}_3$ ceramics within wave number range from 100 to 650 cm^{-1} . With increasing x , some vibrated modes (137 and 220 cm^{-1}) show an apparent blueshift, while the mode (171 cm^{-1}) shifts to the lower wavenumber. Further detailed analysis found that the modes (171 and 220 cm^{-1}) decrease gradually and then vanish at $x=0.2$. Hermet *et al.* supposed that Fe atoms are mainly involved into vibrated range from 152 to 262 cm^{-1} by using first-principles calculation analysis.^{19,20} Therefore, the change in Raman spectra is mainly attributed to the discrepancy of the Fe-O vibrated modes. It is noticed that the ionic radius of Ti^{4+} (0.605 Å) is slightly smaller than that of Fe^{3+} (0.645 Å). The substitution of Fe^{3+} by Ti^{4+} ions in the BFO ceramics induces the entering of Ti^{4+} ions into the Fe-O octahedron. That is to say, the Raman results reveal that Ti^{4+} ions occupy fully the position of Fe^{3+} ion, which is consistent with the results of XRD, see Fig. 1.

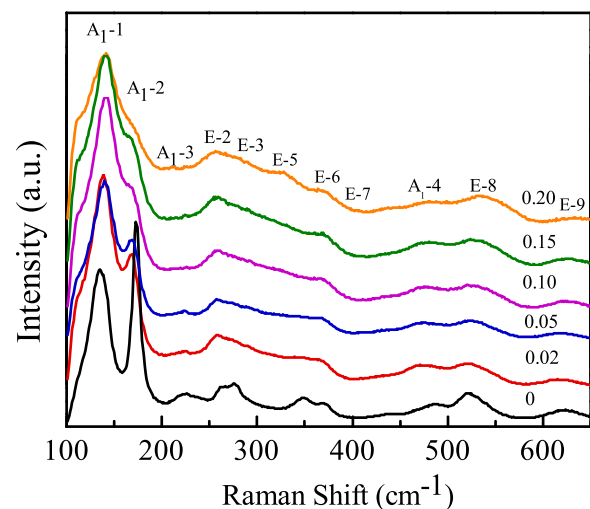


FIG. 2. Raman spectra of the $\text{BiFe}_{1-4x/3}\text{Ti}_x\text{O}_3$ ceramics measured at room temperature with wavenumber range from 200 to 650 cm^{-1} .

The dielectric constant and dielectric loss as a function of frequency at room temperature are shown in Figure 3 for the $\text{BiFe}_{1-4x/3}\text{Ti}_x\text{O}_3$ samples. From Fig. 3(a), It can be seen that the dielectric constant of pure BFO ceramic ($x = 0$) is about 230 at 100 Hz and decreases gradually with increasing frequency. In contrast, the dielectric constant in each Ti-doped sample ($x > 0$) is about 100 at 100 Hz and almost remains unchanged with increasing frequency. Importantly, the dielectric loss, see Fig. 3(b), for each Ti-doped sample decreases significantly in comparison with the one in the pure sample, implying an improvement in the leakage current. Such a result with decreased dielectric constant and dielectric loss has been reported for Ti-substituted BFO ceramics fabricated by other researcher.^{14,18} Gu *et al.*¹⁸ explained the reasons as Fe vacancy-relevant. Actually, the electronic conduction originated from the hopping between Fe^{2+} and Fe^{3+} is suppressed by the Fe vacancy artificially created by a nonstoichiometric formula, which leads to the low dielectric loss in our samples.

Figure 4 shows the magnetization hysteresis (M-H) loops of $\text{BiFe}_{1-4x/3}\text{Ti}_x\text{O}_3$ samples measured at room temperature with a maximum magnetic field of 60 kOe. It is common that the pure BFO ceramic presents a nearly antiferromagnetic behavior. In Ti-doped BFO ceramics, its weak ferromagnetism is improved greatly. With increasing x , the remanent magnetization (M_r) first increases rapidly and then decreases gradually, see the insert of Fig. 4. The maximal M_r of 0.13 emu/g is obtained at $x = 0.05$. It is worth noting that M_r in our nonstoichiometric compositions is larger than the one in stoichiometric $\text{BiFe}_{1-x}\text{Ti}_x\text{O}_3$ ($x = 0-0.35$) ceramics reported by Kumar *et al.*,¹⁴ and consistent with the value reported in other nonstoichiometric compositions such as $\text{BiFe}_{0.9}\text{Ti}_{0.05}\text{O}_3$.¹⁸ Actually, the improved magnetism in Ti-doped BFO ceramic originates from the suppression of the space-modulated antiferromagnetic spin orderings as mentioned in other papers.²¹⁻²⁴ Upon the substitution of magnetic Fe^{3+} ions by nonmagnetic Ti^{4+} ions, the Fe vacancies

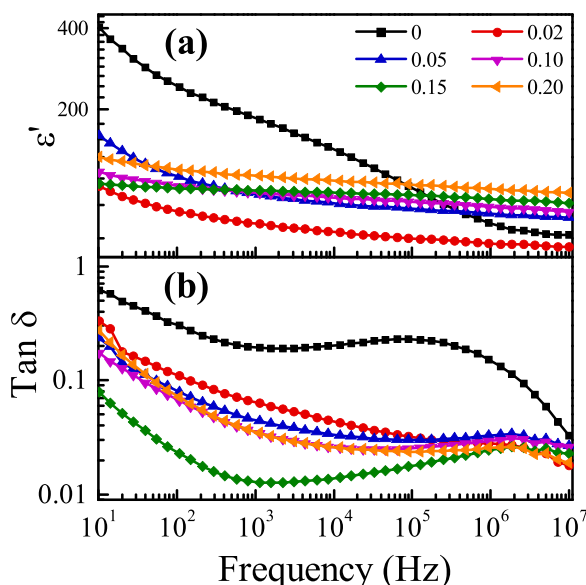


FIG. 3. Frequency dependence of (a) the dielectric constant, ϵ' and (b) dielectric loss, $\text{Tan } \delta$ for the $\text{BiFe}_{1-4x/3}\text{Ti}_x\text{O}_3$ ceramics at room temperature.

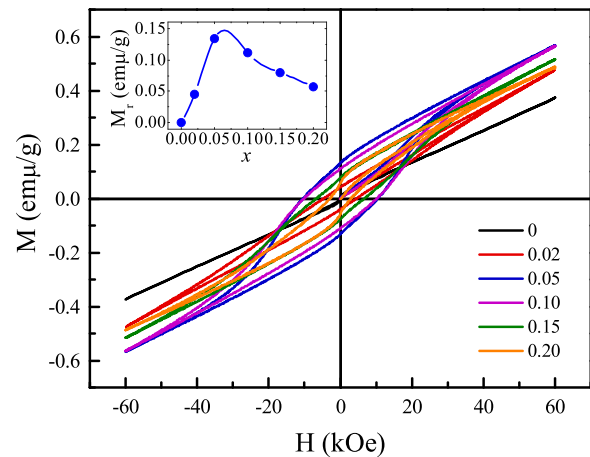


FIG. 4. M-H hysteresis loops for the $\text{BiFe}_{1-4x/3}\text{Ti}_x\text{O}_3$ ceramics at room temperature.

are created by a nonstoichiometric ratio so that the nearest antiparallel spin orderings of Fe^{3+} ions in lattice are broken by nonmagnetic Ti^{4+} ions, in particular, the Fe vacancies. This is the non-cancellation among spin orderings that leads to a net magnetic moment.²⁵ A theoretical calculation on this problem will be given in Sec. IV.

It is noticed that M_r does reduce at relatively high Ti-doped concentration ($x > 0.05$). This phenomenon may attribute to two possible reasons. One is the occurrence of an impure phase as characterized by XRD (Fig. 1). Other is that the Fe vacancies with high concentration may lead to a pinning effect of spin moments as the Fe vacancies correspond to the center of negative charge. Furthermore, the hysteresis loops do not reach saturation even in the high magnetic field of 60 kOe. Similar phenomenon has been reported in doped BFO ceramics.¹⁴⁻¹⁸ Although the magnetism originates from the suppression of the space-modulated spin orderings in BFO, such suppression or destruction of spin cycloid does not change the nature of canting of the antiferromagnetic sublattices.²⁶ In order words, the intrinsic AFM still exists in the doped BFO ceramics. Finally, it is interesting to note that the ferroelectric polarization is not degraded when the magnetism and leakage current is enhanced greatly, implying that their multiferroic behavior should be improved in Ti-doped BFO ceramics through introduction of some Fe vacancies.

In order to clarify the enhanced lattice constant and magnetic moment in Ti-doped BFO ceramic, we used first-principles density functional theory within the projector augmented wave (PAW) method,²⁷ as implemented in the Vienna *Ab initio* Simulation Package (VASP).²⁸ To treat exchange and correlation effects, we use the generalized gradient approximation plus U (GGA+U) method for a better description of the localized transition metal d electrons and a moderate value of $U = 6$ eV leads to a good description of the structural parameters and the ferroelectric polarization in BFO.²⁹ We treated the basis with Bi $5d^{10}6s^26p^3$, Fe $3p^63d^74s^1$, Ti $3p^63d^34s^1$, and O $2s^22p^4$. A kinetic energy cut-off of 500 eV and a Monkhorst-Pack grid of $3 \times 3 \times 3$ k-points were employed to sample the Brillouin zone.

The properties of pure BFO ($x = 0$) with R3c rhombohedral structure were calculated first. The fully relaxed crystal

structure [$a = 5.56 \text{ \AA}$, $\alpha = 59.75^\circ$] with primitive cell in pure BFO structure is in good agreement with the experimental values [$a = 5.63 \text{ \AA}$, $\alpha = 59.35^\circ$]. In order to describe the Ti-doped BFO ceramic with Fe vacancies, we build a $2 \times 2 \times 2$ periodic supercell (80 atoms) based on the optimized primitive cell, in which four of the Fe atoms were replaced by three Ti atoms without considering site configurations, giving rise to a unit cell formula $\text{Bi}_{16}\text{Fe}_{12}\text{Ti}_3\text{O}_{48}$. The Ti-doped BFO system was relaxed fully for the lattice constant and all atoms equilibrium positions until the atomic forces are less than 1 meV/\AA . All calculations are assumed as Rock-salt (*G*-type) AFM ordering because BFO is observed experimentally to be nearly *G*-type AFM configuration.

The calculated structure of Ti-doped BFO shows that the lattice constant [$a = 5.59 \text{ \AA}$, $\alpha = 59.71^\circ$] is larger than that of perfect BFO, and consistent with the result calculated from XRD data, see Fig. 1. The calculated total density of states (DOS) of pure and Ti-doped BFO are shown in Figure 5. It is found that the Ti-doped BFO shows a half-metallic behavior, where the spin-up DOS is metallic, while the spin-down DOS is insulating at Fermi level. These unpaired electrons around the Fe vacancy at the Fermi level are almost completely polarized so that produces a net magnetic moment of $4.02\mu_B$, which is consistent with the experimental data (Fig. 4). Although some electronic states are excited into the Fermi level, the band gap is slightly widened, implying a possible improved leakage current density and ferroelectric polarization. Further analysis shows that the presence of Fe vacancies does not change the local magnetic moment on the Fe sites. The local magnetic moments at the Fe sites are about $\pm 4.3\mu_B$ both in pure and Ti-doped BFO, corresponding to the so-called Fe^{3+} . That is to say that the electron hopping between Fe^{2+} and Fe^{3+} is almost suppressed, indicating the decrease of leakage current density, which is in good agreement with the previously experimentally reported results (Fig. 3(b)). In addition, the enhanced magnetism mainly originates from the suppression of the spatially modulated AFM

spin orderings because the total magnetic moment ($4.02\mu_B$) is almost equal with that of Fe atom ($4.3\mu_B$). Therefore, the calculated results prove that the magnetic moment is enhanced greatly, while the leakage current or ferroelectric polarization is not degraded in Ti-doped BFO ceramic with Fe vacancy.

IV. CONCLUSIONS

Nonstoichiometric $\text{BiFe}_{1-4x/3}\text{Ti}_x\text{O}_3$ ($x = 0-0.2$) have been successfully synthesized. XRD and Raman patterns showed a structure transition from rhombohedral to orthorhombic phases at $x = 0.2$. Dielectric measurements revealed the decrease of dielectric loss in Ti-doped BFO. The magnetic properties were first increased and then decreased with increasing Ti-doped concentration, giving rise to a maximal M_r of 0.13 emu/g at $x = 0.05$. Fe vacancies play a vital role in the suppression of the cycloid AFM spin orderings to enhance the magnetism. Meanwhile, first-principles calculations proved that the Ti-doping does enhance the lattice constants, band gap, and magnetic moment. Both of experiment and theoretical results imply that their multiferroic behavior should be improved in Ti-doped BFO ceramics through introduction of some Fe vacancies because the ferroelectric polarization is not degraded when the magnetism and leakage current are enhanced greatly.

ACKNOWLEDGMENTS

The authors would like to acknowledge the financial assist from the Natural Science Foundation of China (Grant Nos. 51101063, 51072061, and 51031004), the Natural Science Foundation of Guangdong Province of China (No. S2011040003205), and Foundation for High-level Talents in Higher Education of Guangdong, China.

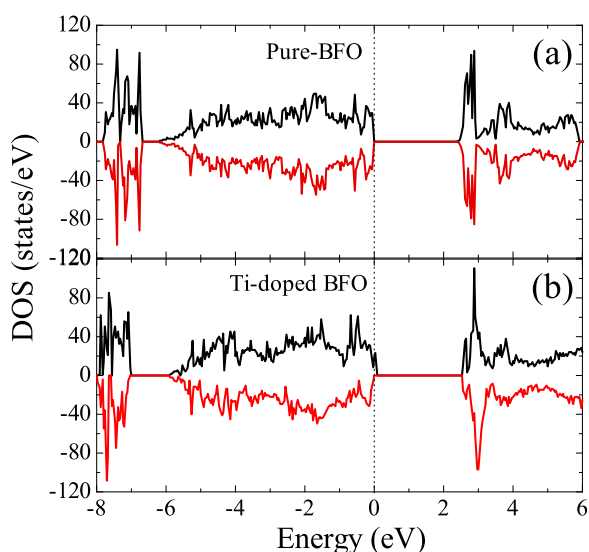


FIG. 5. The total DOS of (a) pure BFO and (b) Ti-doped BFO with formula $\text{Bi}_{16}\text{Fe}_{12}\text{Ti}_3\text{O}_{48}$. The positive (negative) values represent the spin-up (down), respectively. The zero-point energy is the Fermi level.

- ¹S. W. Cheong and M. Mostovoy, *Nat. Mater.* **6**, 13 (2007).
- ²K. F. Wang, J. M. Liu, and Z. F. Ren, *Adv. Phys.* **58**, 321(2009).
- ³J. Wang, J. B. Neaton, H. Zheng, V. Nagarajan, S. B. Ogale, B. Liu, D. Viehland, V. Vaithyanathan, D. G. Schlom, U. V. Waghmare, N. A. Spaldin, K. M. Rabe, M. Wuttig, and R. Ramesh, *Science* **299**, 1719 (2003).
- ⁴R. Ramesh and N. A. Spaldin, *Nat. Mater.* **6**, 21 (2007).
- ⁵J. B. Neaton, C. Ederer, U. V. Waghmare, N. A. Spaldin, and K. M. Rabe, *Phys. Rev. B* **71**, 014113 (2005).
- ⁶X. Qi, J. Dho, R. Tomov, M. G. Blamire, and J. L. MacManus-Driscoll, *Appl. Phys. Lett.* **86**, 062903 (2005).
- ⁷F. Bai, J. Wang, M. Wuttig, J. F. Li, N. Wang, A. P. Pyatakov, A. K. Zvezdin, L. E. Cross, and D. Viehland, *Appl. Phys. Lett.* **86**, 032511 (2005).
- ⁸J. Wu, G. Kang, and J. Wang, *Appl. Phys. Lett.* **95**, 192901 (2009).
- ⁹J. F. Scott and M. Dawber, *Appl. Phys. Lett.* **76**, 3801 (2000).
- ¹⁰V. V. Lazenka, A. F. Ravinski, I. I. Makoed, J. Vanacken, G. Zhang, and V. V. Moshchalkov, *J. Appl. Phys.* **111**, 123916 (2012).
- ¹¹M. M. Kumar, V. R. Palkar, K. Srinivas, and S. V. Suryanarayana, *Appl. Phys. Lett.* **76**, 2764 (2000).
- ¹²V. R. Palkar, D. C. Kundaliya, and S. K. Malik, *J. Appl. Phys.* **93**, 4337 (2003).
- ¹³S. Zhang, L. Wang, Y. Chen, D. L. Wang, Y. B. Yao, and Y. W. Ma, *J. Appl. Phys.* **111**, 074105 (2012).
- ¹⁴M. Kumar and K. L. Yadav, *Appl. Phys. Lett.* **91**, 112911 (2007).
- ¹⁵V. R. Palkar, S. K. Malik, S. Bhattacharya, and D. C. Kundaliya, *Phys. Rev. B* **69**, 212102 (2004).
- ¹⁶G. L. Yuan, S. W. Or, J. M. Liu, and Z. G. Liu, *Appl. Phys. Lett.* **89**, 052905 (2006).
- ¹⁷N. Wang, J. Cheng, A. Pyatakov, A. K. Zvezdin, J. F. Li, L. E. Cross, and D. Viehland, *Phys. Rev. B* **72**, 104434 (2005).

- ¹⁸Y. H. Gu, Y. Wang, F. Chen, H. L. W. Chan, and W. P. Chen, *J. Appl. Phys.* **108**, 094112 (2010).
- ¹⁹P. Hermet, M. Goffinet, J. Kreisel, and P. Ghosez, *Phys. Rev. B* **75**, 220102 (2007).
- ²⁰S. T. Zhang, Y. Zhang, M. H. Lu, C. L. Du, Y. F. Chen, Z. G. Liu, Y. Y. Zhu, N. B. Ming, and X. Q. Pan, *Appl. Phys. Lett.* **88**, 162901 (2006).
- ²¹P. Li, Y. H. Lin, and C. W. Nan, *J. Appl. Phys.* **110**, 033922 (2011).
- ²²A. Agarwal and S. Sanghi, *J. Appl. Phys.* **110**, 073909 (2011).
- ²³J. M. D. Coey, M. Venkatesan, and C. B. Fitzgerald, *Nat. Mater.* **4**, 173 (2005).
- ²⁴J. Wei, R. Haumont, R. Jarrier, P. Berhtet, and B. Dkhil, *Appl. Phys. Lett.* **96**, 102509 (2010).
- ²⁵Y. H. Lin, Q. H. Jiang, Y. Wang, and C. W. Nan, *Appl. Phys. Lett.* **90**, 172507 (2007).
- ²⁶G. Kresse and J. Furthmuller, *Phys. Rev. B* **54**, 11169 (1996).
- ²⁷P. E. Blöchl, *Phys. Rev. B* **50**, 17953 (1994).
- ²⁸Z. Zhang, P. Wu, L. Chen, and J. Wang, *Appl. Phys. Lett.* **96**, 232906 (2010).
- ²⁹F. Kubel and H. Schmid, *Acta Crystallogr., Sect. B: Struct. Sci.* **46**, 698 (1990).